# การจำลองเชิงตัวเลขของการถ่ายเทความร้อนและการไหลในเจ็ตพุ่งชนโดยใช้ของไหลนาโนไททาเนียมออกไซด์

# Numerical simulation of heat transfer and fluid flow in a confined jet impingement using water-$TiO_2$ nanofluid

คมกฤษณ์ ชัยโย[1*]
Khomgris Chaiyo[1*]

**Received**: 18 May 2021 ; **Revised**: 30 July 2021 ; **Accepted**: 16 August 2021

## บทคัดย่อ

งานวิจัยนี้ได้นำการจำลองเชิงตัวเลขมาใช้เพื่อศึกษาลักษณะการถ่ายเทความร้อนและการไหลในเจ็ตของไหลนาโนพุ่งชนแบบราบเรียบที่มีพื้นผิวร้อนอุณหภูมิคงที่ด้วยแบบจำลองเดี่ยว ระเบียบวิธีไฟไนต์วอลุมถูกใช้เพื่อหาผลเฉลยของสมการควบคุม การถ่ายเทความร้อนและการไหลโดยใช้ของไหลนาโนไททาเนียมออกไซด์ ($TiO_2$) เป็นสารทำงานที่มีความเข้มข้นโดยปริมาตรอยู่ระหว่าง 0% ถึง 4% การคำนวณได้ทำการศึกษาถึงผลกระทบของการเปลี่ยนแปลงค่าเข้มข้นโดยปริมาตรของอนุภาคนาโน ค่าอัตราส่วนความสูง H ต่อความกว้างของทางไหลเข้า B และค่าเรย์โนลด์นัมเบอร์ ผลการคำนวณที่ได้พบว่าการถ่ายเทความร้อนเพิ่มขึ้นตามค่าเข้มข้นโดยปริมาตรของอนุภาคนาโนและและค่าเรย์โนลด์นัมเบอร์เมื่อพิจารณาจากทั้งค่านัสเซิลนัมเบอร์ ณ ตำแหน่งใดๆ และค่านัสเซิลนัมเบอร์เฉลี่ย แต่สำหรับกรณีของการเปลี่ยนแปลงค่าอัตราส่วนความสูงต่อความกว้างของทางไหลเข้าให้เพิ่มขึ้นสูงในช่วงระหว่าง 1 ถึง 4 นั้นทำให้อัตราการถ่ายเทความร้อนมีค่าลดลง

**คำสำคัญ:** การพุ่งชนระบายความร้อน การส่งเสริมการถ่ายเทความร้อน ของไหลนาโน อนุภาคนาโนไททาเนียมออกไซด์

## Abstract

This article presents a numerical investigation of heat transfer and fluid flow of a confined plane laminar nanofluid jet impingement on an isothermal heated surface using a single-phase model. The finite volume method was used for the solution of resulting governing equations. $TiO_2$ nanoparticles dispersed in water with volumetric concentrations ranging between 0 and 4% were used as working fluid for simulating the heat transfer and fluid flow of nanofluid jet impingement. The influences of volumetric concentration of nanoparticles, nozzle-to-impingement surfaces (aspect ratio H/B, where H is the distance between the nozzle and the impingement surface and B is jet width) and Reynolds number were examined and discussed in detail. The results indicated that the volumetric concentration of nanoparticles and Reynolds number enhanced heat transfer when considered in terms of the local and average Nusselt number. However, heat transfer deteriorated whereas increasing aspect ratio ranged from 1 to 4.

**Keywords:** impinging jet, heat transfer enhancement, nanofluids, $TiO_2$ nanoparticles

[1] อาจารย์, ภาควิชาวิศวกรรมเครื่องกล คณะวิศวกรรมศาสตร์ กำแพงแสน มหาวิทยาลัยเกษตรศาสตร์ วิทยาเขตกำแพงแสน นครปฐม 73140
[1] Lecturer, Department of Mechanical Engineering, Faculty of Engineering at Kamphaengsaen, Kasetsart University, Kamphaengsaen Campus, Nakhonpathom, 73140
* E-mail: khomgris.c@ku.th

## Introduction

Impinging jets provide an effective and flexible way to transfer energy or mass in industrial applications. A directed liquid or gaseous flow released against a surface can efficiently transfer large amounts of thermal energy or mass between the surface and the fluid. Heat transfer applications include cooling of stock material during material forming processes, heat treatment (Ferrari *et al.*, 2003), cooling of electronic components, heating of optical surfaces for defogging, cooling of turbine components, cooling of critical machinery structures, and many other industrial processes (Zuckerman & Lior, 2006).

Nanofluids are a suspension of very fine solid particles (nanoparticles) with length scales of 1–100 nm, dispersed in base fluids such as water, engine oil, and ethylene glycol (Choi & Eastman, 1995). Due to the enhancement in thermal conductivity and heat transfer provided by nano-fluids compared to classical heat transfer fluids, nanofluids have become highly significant for a wide range of engineering applications which require high heat dissipation rates. Such applications include heat exchangers (Venkitaraj *et al.*, 1995) and cooling of electronic components which suffers from a high heat generation (Selvakumar & Suresh, 2012). Integrating nanofluids with impinging jets is considered a promising technique that can overcome the challenges of heat removal (Abdelrehim *et al.*, 2019).

The existing types of nanoparticles that are used suspended in fluids can be classified as follows: (1) some advanced structural materials with highest thermal conductivity such as graphene, CNTs, diamond etc. (2) some metallic simples with high thermal conductivity such as, Au, Ag, Cu, Al, Fe, etc. (3) some metal or non-metallic compounds such as CuO, $Al_2O_3$, $TiO_2$, ZnO, SiC, $SiO_2$ etc. After comprehensive analysis and comparisons, $TiO_2$ nanofluid is a common type of nanofluid without extremely high thermal conductivity as found with some precious materials, for instance CNTs or Graphene based nanofluid. $TiO_2$ nanofluid has some special features and unique points compared to other types. It is thought that $TiO_2$ is one of the best materials for practical application since $TiO_2$ exhibits several more comprehensive and reliable superiorities compared to other materials. Firstly, $TiO_2$ has been extensively used in the fields of cosmetics, printing and purification without any toxicity, which is an essential requirement for largescale application. Secondly, $TiO_2$ nanoparticles have been produced in large industrial scale, which makes them economical and appropriate for high-volume applications in thermal fluid fields. Thirdly, $TiO_2$ nanoparticles have outstanding chemical stability, acid and caustic corrosion resistance as well as high temperature resistance. Finally, $TiO_2$ nanoparticles have shown excellent dispersivity in both polar and non-polar basefluids as reported extensively in the literature, and it can be further improved by adding some specialized dispersants (Yang & Du, 2017).

Several studies have investigated numerically, utilizing the single-phase model under a laminar flow regime using water-$Al_2O_3$ nanofluids. A confined impinging slot jets working with pure water or water-$Al_2O_3$ based nanofluids was numerically presented. The flow is laminar and a constant uniform temperature is applied on the target surface. The single-phase model approach was adopted in order to describe the nanofluid behavior and different particle volume concentrations. The results demonstrated that the stagnation point, the local and averaged Nusselt number values were increased when increasing particle concentrations and Reynolds numbers increased. The required pumping power ratio also increased with growing particle concentration (Manca *et al.*, 2016).

The single-and two-phase models of water-$Al_2O_3$ nanofluids on the hydrodynamic and heat transfer characteristics of a confined single impinging jet were studied. A laminar flow was considered with a constant heat flux on the targeted surface. The effects of Reynolds number, jet height ratio, and nanoparticle volume fraction on the local and the averaged Nusselt number were determined. The results demonstrated that the two-phase model exhibited higher values of local and averaged Nusselt number with a maximum enhancement of 150% at H/W=4 and $\phi$=4% while the single phase model showed twice the pumping power obtained by the two-phase model (Abdelrehim *et al.*, 2019).

The thermal and fluid dynamic behavior of a confined two-dimensional steady laminar nanofluid jet impinging on a horizontal plate embedded with five

discrete heating elements subjected to a constant surface heat flux was studied for a range of Reynolds number from 100 to 400. The results indicated that variation of inlet Reynolds number produced a significant change of the flow and heat transfer characteristics in the domain. Increasing the nanoparticle concentration from 0% to 4% resulted in discernible change in equivalent Re and Pr caused by the modification of dynamic viscosity, effective density, thermal conductivity, and specific heat of the base fluid. Substantial influence of Re was evident on Eckert number and pumping power. Eckert number was decreased whereas pumping power was increased with the growth of Re (Mookherjee *et al.*, 2020).

Analysis of nanofluids flowing through microchannel heat sinks was experimentally investigated. The fluid flow and convective heat transfer in different microchannel heat sinks using $Al_2O_3$ and $TiO_2$ nanofluids were studied. The results demonstrated that the thermal conductivity and dynamic viscosity of nanofluids were enhanced with the increase of volume fraction. As a result, $TiO_2$ nanofluids had a better behavior on thermal conductivity than $Al_2O_3$ nanofluids. However $Al_2O_3$ nanofluids achieved a greater enhancement of heat transfer in terms of averaged heat transfer coefficient compared with $TiO_2$ nanofluids, specifically for the volume fraction of 1.0% (Xia *et al.*, 2016).

Nevertheless, $TiO_2$ nanoparticles are more environment friendly and economically friendly (Yang & Du, 2017 ; Mosurkal *et al.*, 2008) compared to $Al_2O_3$ nanoparticles. Hence it is better to use water-$TiO_2$ nanofluid in real life applications. These reasons are to contribute of this research using water-$TiO_2$ nanofluid as working fluid. Furthermore, several numerical studies are currently available on the numerical study of laminar heat transfer and fluid flow of nanofluids impingement jet utilizing the single-phase model, but there have been fewer studies on water-$TiO_2$ nanofluid as working fluid.

The objective of this study was to numerical evaluate the results of heat transfer and fluid flow obtained by the single-phase model in a confined plane laminar jet impingement using water-$TiO_2$ nanofluid to cool the isothermal heated surface. The latest viscosity of water-$TiO_2$ nanofluid equation was applied by fitting the experimental data. Furthermore, the influence of volumetric concentration of nanoparticles, aspect ratio and the jet inlet Reynolds number (varied from Re=100 to 200, the flow is considered to be laminar (Manca *et al.*, 2016 ; Mookherjee *et al.*, 2020) were investigated.

## Methods

### A. Problem description

A schematic diagram of the two-dimensional confined impinging jet is shown in Figure 1. The jet width is B, the distance between the nozzle and the impingement surface (channel height) is H, and L represent the surface length. The jet impinges over the isothermal impingement surface while jet inlet temperature is taken as 293 K. The length of the isothermal impingement surface (heated surface) to the width of the impinging jet is fixed at L/B=50, this isothermal impingement has a constant temperature of 313 K. The confinement surface is adiabatic. The aspect ratios (H/B) ranged from 1 to 4 to study the confining effect, and the flow is considered laminar with Re varying from 100 to 200. The working fluid is water-$TiO_2$ nanofluid with the volumetric concentration of nanoparticles ranged from 0 to 4%. The flow of the impinging jet is assumed to be steady, two-dimensional, laminar and incompressible. The body forces are neglected and the fluid properties are assumed to be independent of temperature. Brownian motion and thermophoretic diffusions of the nanoparticles do not have any significant effect on convection heat transfer for the percentage of nanoparticle concentration considered in this study.

### B. Thermophysical properties of nanofluids

The numerical simulations were performed using water-$TiO_2$ nanofluid and the nanoparticle concentrations considered in the present analysis were 0%, 1%, 2%, 3% and 4%. The thermophysical properties of pure water and $TiO_2$ are given in Table 1 (Rohsenow *et al.*, 1998). When the single-phase model was adopted in the present work as nanofluids with small nanoparticle volume concentration can be considered as Newtonian fluids for small temperature jumps (Mookherjee *et al.*, 2020). The density and the specific heat of the nanofluids were evaluated using the formula developed for conventional solid–liquid mixtures as follows:

$$\rho_{nf} = (1-\phi)\rho_{bf} + \phi\rho_p \quad (1)$$

$$(\rho c_p)_{nf} = (1-\phi)(\rho c_p)_{bf} + \phi(\rho c_p)_p \quad (2)$$

where $\phi$, $p_{bf}$, $P_p$, $C_{p,bf}$ and $C_p$ are the volumetric concentration of nanoparticles, density of the base fluid, density of the nanoparticles, specific heat of the base fluid, and the specific heat of the nanoparticles, respectively. The thermal conductivity of water-$TiO_2$ nanofluid was found by fitting measurement data as (He *et al*., 2009).

$$k_{nf} = k_{bf}(125.6\phi^2 + 4.82\phi + 1.0) \quad (3)$$

where $k_{nf}$, $k_{bf}$ is the thermal conductivity of nanofluid and base fluid, respectively.

The following equation of the viscosity of water-$TiO_2$ nanofluid was created to fit the experimental data (Alkasmoul *et al*., 2018).

$$\mu_{nf} = \mu_{bf}(25.17\phi^2 + 29.562\phi + 1.0) \quad (4)$$

where $\mu_{nf}$, $\mu_{bf}$ is the viscosity of nanofluid and base fluid, respectively.

**C. Governing equations**

In the present study, flows were assumed to be steady and incompressible. The governing equations include the conservation equations of mass, momentum, and energy, and can be written in the two-dimensional Cartesian coordinate system form as follows:

Continuity:

$$\frac{\partial}{\partial x_i}(\rho u_i) = 0 \quad (5)$$

Momentum:

$$\frac{\partial}{\partial x_j}(\rho u_j u_i) = -\frac{\partial p}{\partial x_i} + \frac{\partial}{\partial x_j}\left(\mu \frac{\partial u_i}{\partial x_j}\right) \quad (6)$$

Energy:

$$\frac{\partial}{\partial x_j}(\rho u_j T) = \frac{\partial}{\partial x_j}\left(\frac{\mu}{Pr}\frac{\partial T}{\partial x_j}\right) \quad (7)$$

where $u_i$ is velocities in the streamwise and crosswise directions respectively, $T$ is temperature, and $p$ is pressure.

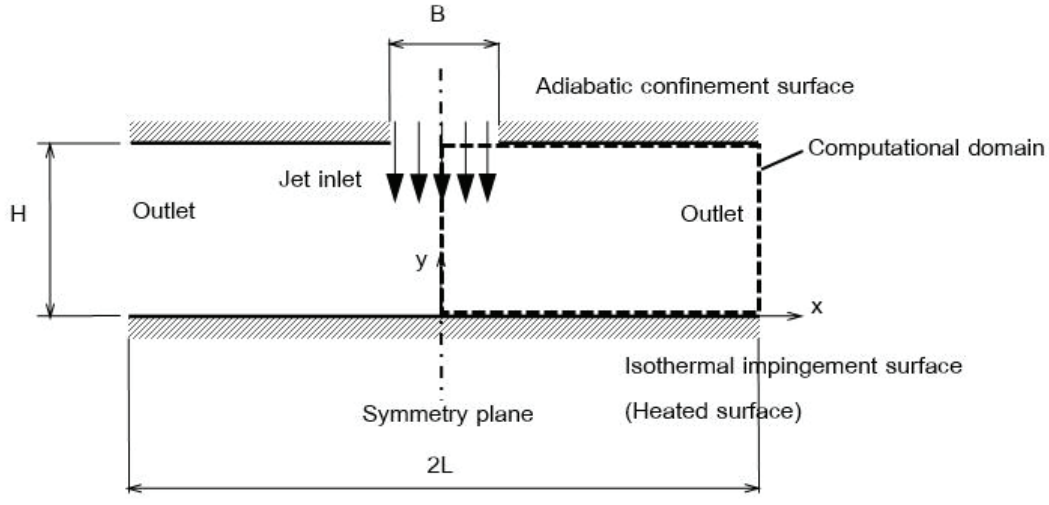


**Figure 1** The two-dimensional confined impinging jet

**Table 1** Thermophysical properties of pure water and $TiO_2$ particles at T = 293 K used in the computations

| Material | Density | Heat capacity | Viscosity | Thermal conductivity |
|---|---|---|---|---|
| | $p$ (kg/m$^3$) | $C_p$ (J/kg.K) | $\mu$ (Pa.s) | $\lambda$ (W/m.K) |
| $TiO_2$ | 4170 | 711 | - | 11.8 |
| Water | 998.2 | 4182 | 993x10$^{-6}$ | 0.597 |

**D. Numerical solution procedure**

The computations have been performed with in-house developed computational code. The governing equations were solved using the finite volume method (Patankar, 1980). This scheme solved discretized versions of all equations with a non-uniform a staggered grids. The principle of mass-flux continuity was improved indirectly via the solution of pressure-correction equations according to SIMPLE algorithm (Patankar, 1980). The convergence was judged by monitoring the magnitude of the absolute residual sources of mass, momentum and energy, normalized by the respective inlet fluxes. The solution was taken as having converged when all above residuals fell below 0.0001%.

The geometry of a two-dimensional plane impinging jet consists of the jet stream, impinging and confinement surfaces as shown in Figure 1. Therefore, computational boundaries involved were inlet, outlet, axis of symmetry and solid walls (impingement and confinement surfaces).

At the inlet, the jet temperature is given at 293 K. The jet stream had an almost uniform velocity profile. The Reynolds number was calculated based on jet width and mean centerline velocity as:

$$\mathrm{Re} = \frac{\rho v_0 B}{\mu} \tag{8}$$

Next, the outlet boundary was placed at which is sufficiently far away from the main region of interest. At this boundary streamwise gradients of all variables were set to zero. Then along the axis of symmetry, the normal velocity component and the normal gradients of other variables were set to zero.

Finally, solid walls included impingement and confinement surfaces. Also the impingement surface was considered isothermal, the impingement surface temperature $T_w$ is given at 313 K and the confinement surface is adiabatic wall, respectively. The Nusselt number, $Nu$ is defined as:

$$\mathrm{Nu} = \frac{-\left(\frac{\partial T}{\partial y}\right)_w B}{T_w - T_y} \tag{9}$$

Before proceeding to the discussion of the predicted results, it will beneficial to focus first on the effect of the grid density on the solution. Figure 2 shows the computational grid 246x30 at distance x/B=50 and H/B=4. Grid clustering is applied near the impingement surface and at the confinement surface. The grid-independency of the solutions was examined using three different grid sizes consisting of 7380 (246x30), 17900 (358x50), 59040 (492x120) and 121880 (554x220) on the model H/B=4 at Re=100 with water as working fluid. The results on the third grid 492x120 can be considered as being grid-independent results because the refinement from the grid 492x120 to grid 554x220 produces the stagnation point Nusselt number difference too small as shown in Figure 3.

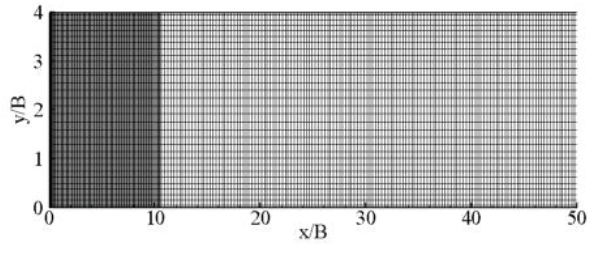


**Figure 2** Sample of computational grid 246x30

## Results and Discussion

The numerical results of a two-dimensional laminar confined jet of watet-$TiO_2$-water nanofluid impinging on a stationary isothermal heated surface were investigated. Data presented include the influence of volume concentration, aspect ratio and Reynolds number.

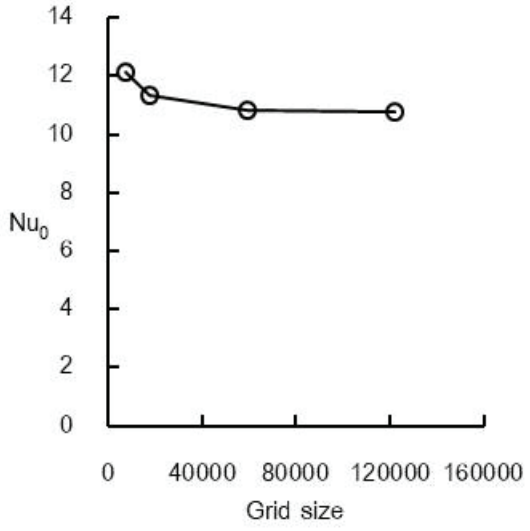


**Figure 3** Grid independence test results in terms of stagnation point Nusselt number

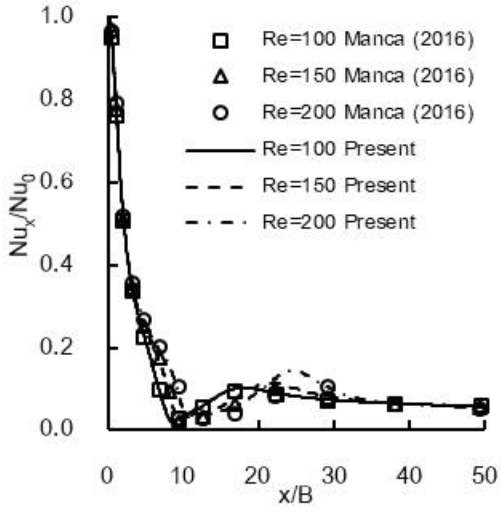


**Figure 4** Validation of local Nusselt number $Nu_x$ profiles are scaled with the stagnation point Nusselt number $Nu_0$ for H/B=4

### A. Numerical validation

In order to verify the developed computational code, the simulation results including the stagnation point Nusselt number and the local Nusselt number along the impingement surface for H/B=4 were compared with the previously obtained numerical data. The present numerical results are in good agreement with the results of Manca *et al.* (2018) as shown in Table 2 and Figure 4, respectively.

**Table 2** Validation of the stagnation point Nusselt number for H/B=4 and $\phi$=0%

| Re | $Nu_0/Pr^{1/3}$ | | %Error |
|---|---|---|---|
| | Manca (2016) | Present simulation | |
| 100 | 5.66 | 5.67 | 0.18% |
| 150 | 7.02 | 7.07 | 0.71% |
| 200 | 8.04 | 8.18 | 1.71% |

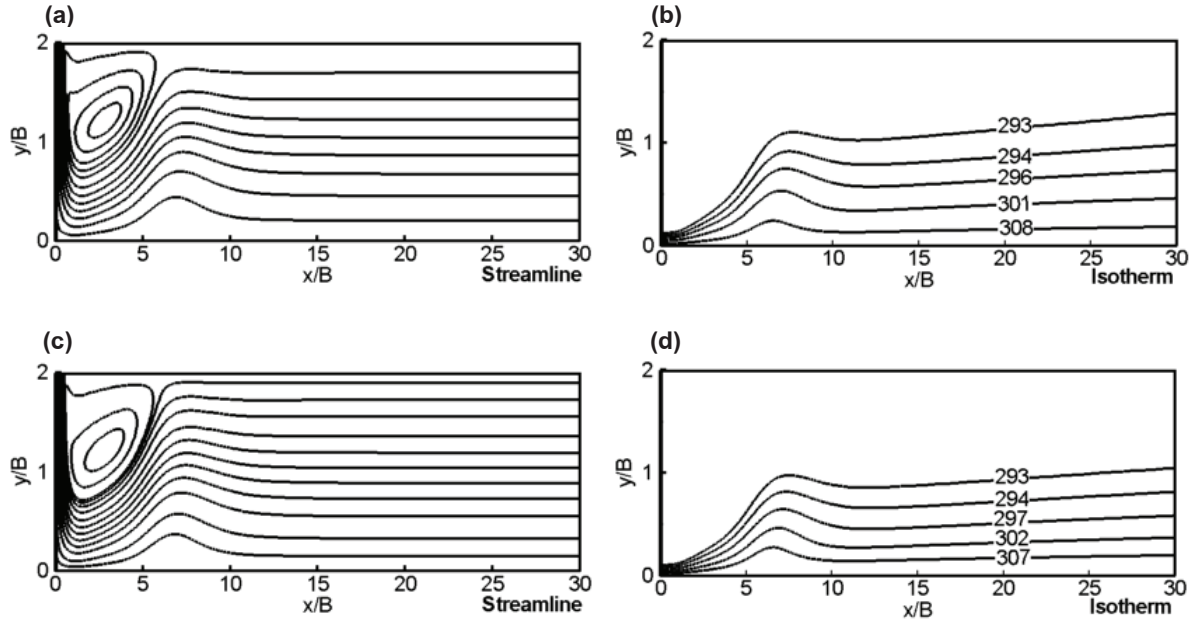


**Figure 5** Streamlines and isotherms for H/B=2 and Re=150 (not to scale) (a) Streamline $\phi$=0%, (b) Isotherm $\phi$=0%, (c) Streamline $\phi$=4%, (d) Isotherm $\phi$=4%

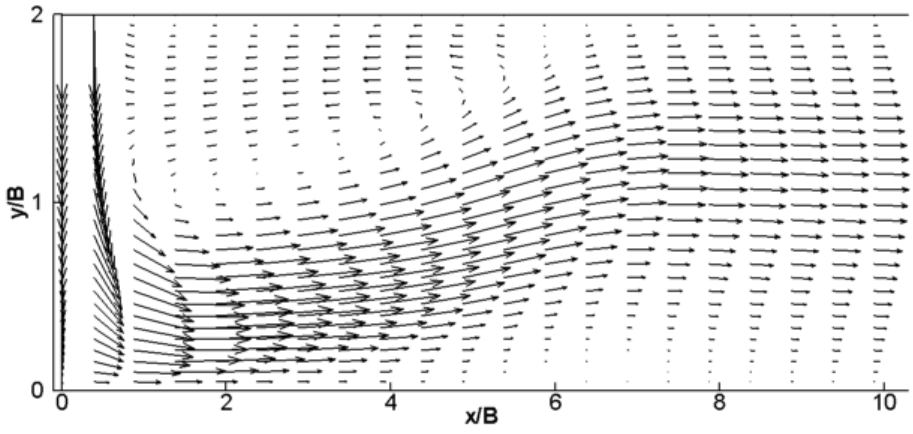


**Figure 6** Velocity vectors for H/B=2, Re=150 and $\phi$=4% (not to scale)

**B. Influence of volumetric concentration**

The numerical results of heat transfer and fluid flow were investigated at different volumetric concentrations of nanoparticles with values of $\phi$= 0%, 1%, 2%, 3% and 4% for H/B=2. Figure 5 illustrates streamlines and isotherms in the case of H/B=2 and Re=150 for volume concentration $\phi$=0% and 4%, respectively.

The development of a vortex is generated by the impinging jet because of jet entrainment, confining effects, and isothermal confinement surface. It is seen that a vortex is generated in the immediate vicinity of the jet. The main jet stream impinges on the target isothermal heated impingement surface, gets deflected, and then flows downstream in a meandering path in between the recirculation and the impingement surface toward the outlet. Similar streamline and isotherm trends were observed for two volumetric concentration of nanoparticles. Furthermore, the velocity vectors for H/B=2, Re=150 and $\phi$=4% are shown in Figure 6.

Figure 7 shows the stagnation point Nulsselt number ($Nu_0$) profiles for various volume concentrations and different Reynolds numbers. It is observed that the increased volume concentration, the $Nu_0$ is increased due to increasing thermal conductivity.

Additionally, Figure 8 demonstrates local Nusselt number (Nu) distribution along the impingement surface for H/B=2 and Re=150 at various volume concentrations. It is observed that for increased volumetric concentration of nanoparticles, the values of Nu is increased.

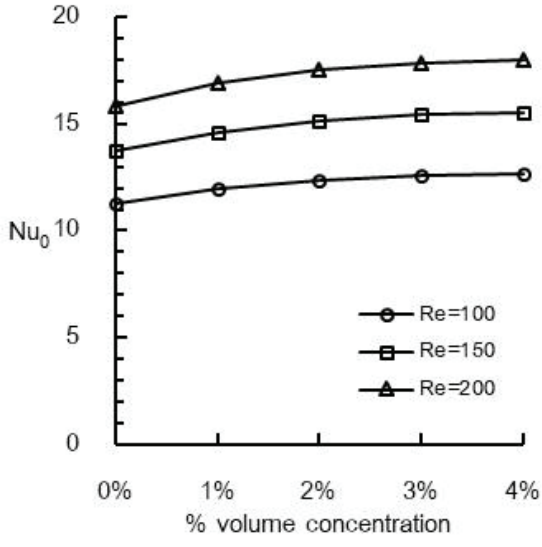


**Figure 7** Stagnation point Nusselt number profiles at different volume concentrations and Re numbers for H/B=2

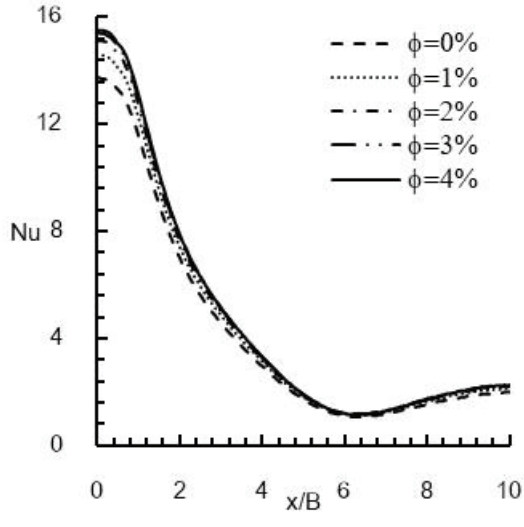


**Figure 8** Local Nulsselt number distribution along the impingement surface for H/B=2 and Re=150

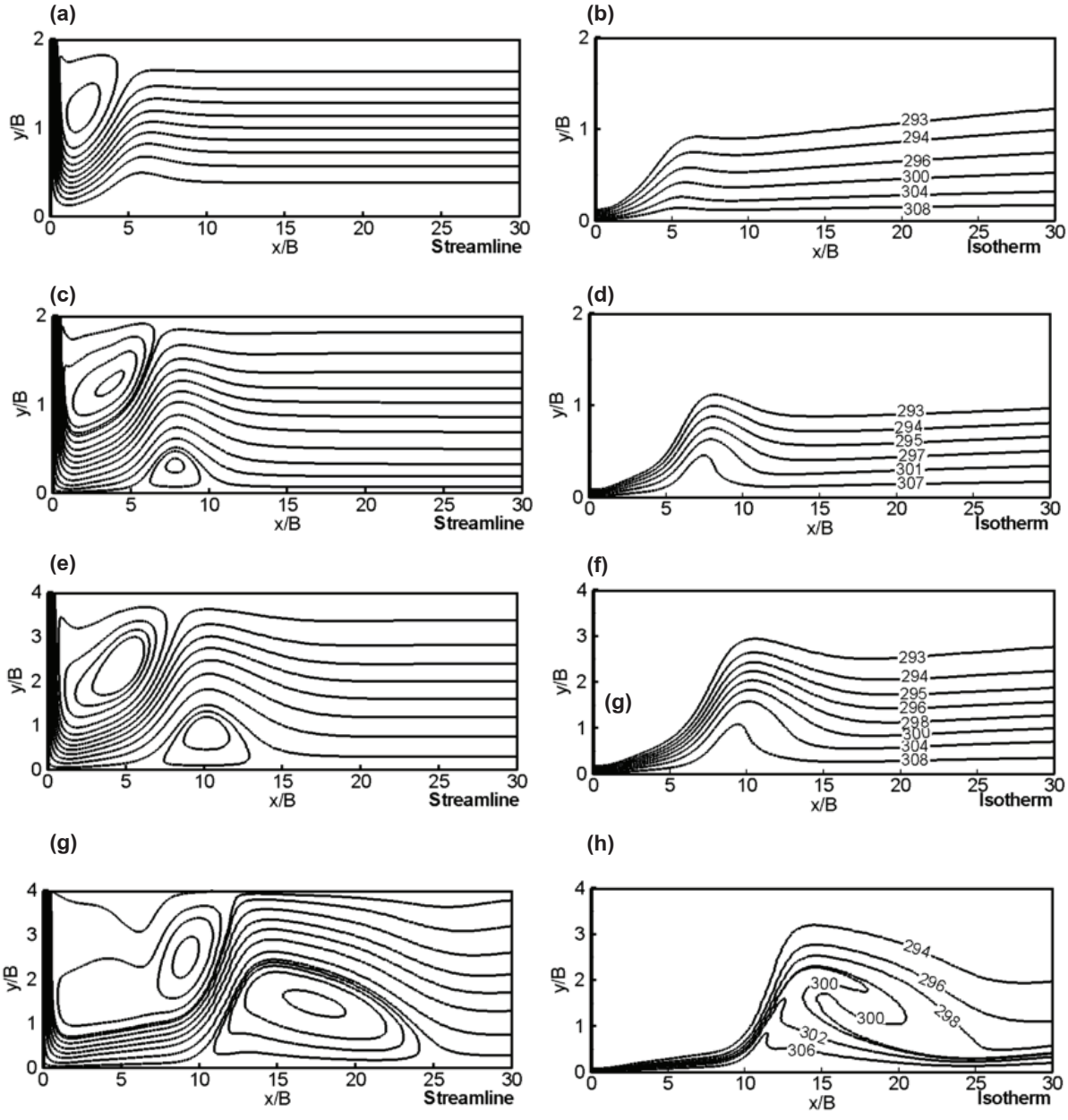


**Figure 9** Streamlines and isotherms at different aspect ratios H/B and Re numbers, $\phi$=4% (not to scale)
(a) Streamline at H/B=2 Re=100, (b) Isotherm at H/B=2 Re=100
(c) Streamline at H/B=2 Re=200, (d) Isotherm at H/B=2 Re=200
(e) Streamline at H/B=4 Re=100, (f) Isotherm at H/B=4 Re=100
(g) Streamline at H/B=4 Re=200, (h) Isotherm at H/B=4 Re=200

**C. Influence of aspect ratio**

Figure 9 shows the streamlines and isotherms when H/B=2 and 4 at Re=100 and 200. At H/B=2 and Re=100, a primary vortex is only generated below the jet. However, at H/B=4, and Re=100, 200, both a primary and a secondary vortices are generated as displayed in Figures 9 (e) and 8 (g).

Figure 10 shows that as H/B is increased, local Nusselt number is decreased due to the secondary vortex. The maximum of Nu is at the stagnation point and then Nu is dramatically decreased along the isothermal impingement surface. This is because increased thickness of the thermal boundary layer and decreased local velocity profile due to the velocity boundary layer.

Furthermore, Figure 11 illustrates stagnation point Nusselt number profiles and Figure 12 demonstrates average Nusselt number profiles in case of $\phi$=0% and 4% at Re=150, respectively. It is found that both $Nu_0$ and $Nu_{avg}$ decreased with increasing H/B.

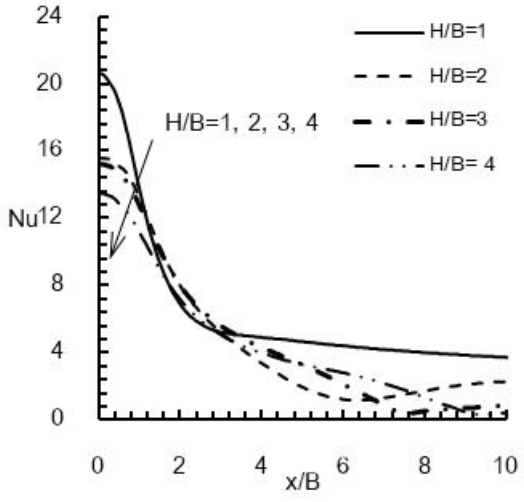


**Figure 10** Local Nusselt number distribution along the impingement surface for $\phi$=4% and Re=150 at different aspect ratio

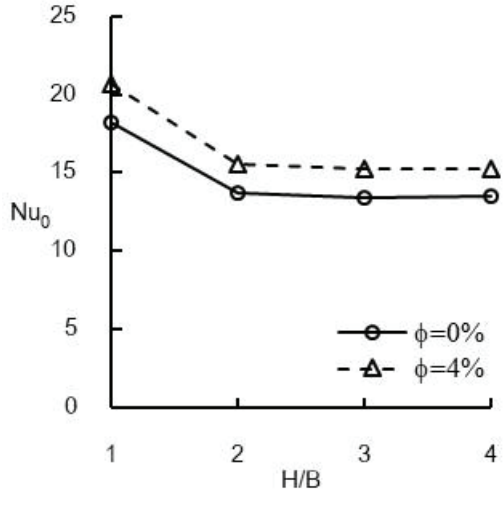


**Figure 11** Stagnation point Nulsselt number profiles for $\phi$=4% and Re=150 at different aspect ratios

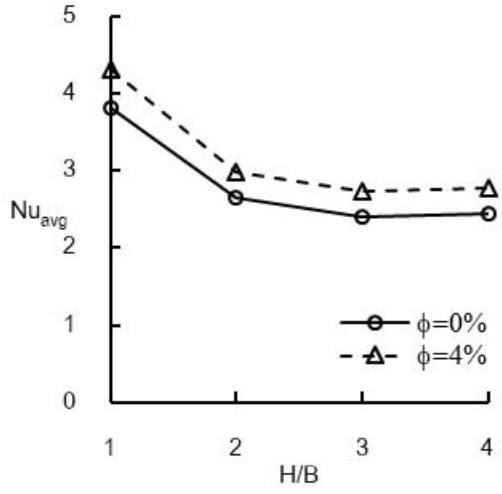


**Figure 12** Average Nulsselt number profiles for $\phi$=4% and Re=150 at different aspect ratios

### D. Influence of Reynolds number

When Reynolds number was increased, the size of both vortices were increased, and the secondary vortex was moved towards downstream. The influence of Re on the heat transfer can be clarified as shown in Figures 9 (f) and 9 (h). Increasing Re leads to increase the heat transfer due to increasing temperature gradient at the isothermal impingement surface. Additionally, the influence of Re on the heat transfer can also be seen in terms of Nu, $Nu_0$, and $Nu_{avg}$ as displayed in Figures 13, 14, and 15, respectively ; these Nusselt number profiles are rise with increasing Re.

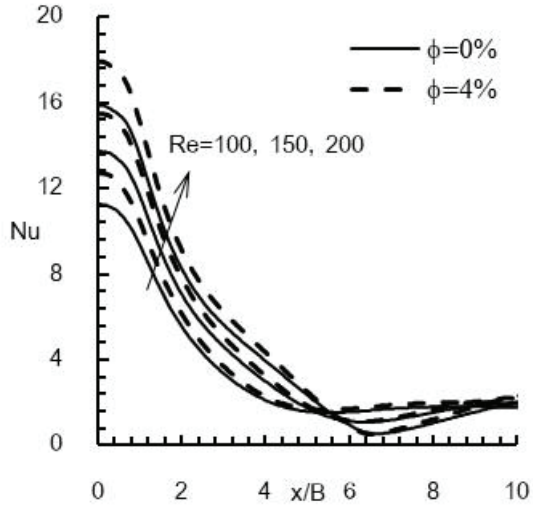


**Figure 13** Local Nulsselt number distribution along the impingement surface for various Re numbers at H/B=2 and $\phi$=4%

## Conclusion

The laminar heat transfer and fluid flow of nanofluids in a confined plane jet impingement were numerically investigated using the single-phase model. The performance of the present simulation of jet impingement flow was evaluated against previous numerical data that was found to produce good predictions of the local Nusselt number along the impingement surface and the stagnation point Nusselt number. The influences of volumetric concentration of nanoparticles, aspect ratio and Reynolds number are examined in detail. The major findings can be summarized as follows:

(1) The volumetric concentration of nanoparticles ranging from 0 to 4% increase the heat transfer in terms of the local and the stagnation Nusselt numbers. Similarly, the Reynolds number varied from 100 to 200 enhance these Nusselt numbers.

(2) However, aspect ratio ranges from 1 to 4 and decrease the local, the stagnation, and average Nusselt numbers.

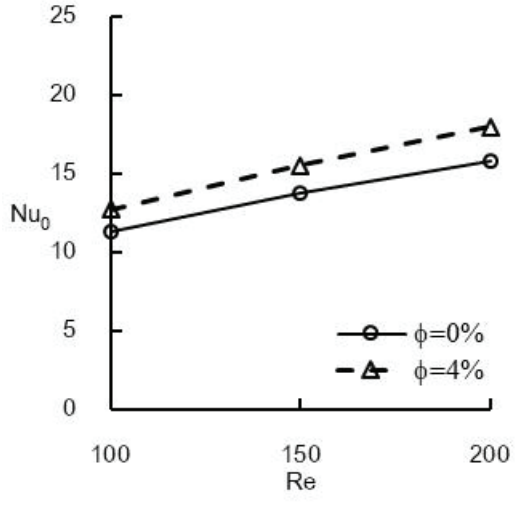


**Figure 14** Stagnation point Nulsselt number profiles for various Re numbers at H/B=2 and $\phi$=4%

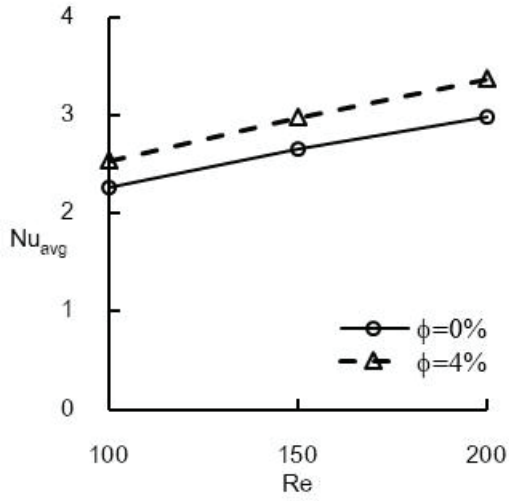


**Figure 15** Average Nulsselt number profiles for various Re numbers at H/B=2 and $\phi$=4%

## Acknowledgment

The author gratefully acknowledges the Faculty of Engineering at Kamphaengsaen, Kasetsart University, Kamphaengsaen Campus, Nakhonpathom for supporting this research.

## References

Abdelrehim, O., Khater, A., Mohamad, A.A. & Radwan, A. (2019). Two-phase simulation of nanofluid in a confined single impinging jet. *Case Stud Therm Eng, 14*, 100423.

Alkasmoul, F.S., Al-Asadi, M.T., Myers, T.G., Thompson, H.M. & Wilson, M.C.T. (2018). A practical evaluation of the performance of $Al_2O_3$-water, $TiO_2$-water and CuO-water nanofluids for convective cooling. *Int J Heat Mass Tran, 126*, 639–651.

Choi, S.U.S. & Eastman, J.A. (1995). Enhancing thermal conductivity of fluids with nanoparticles. *ASME Int Mech Eng Congr Expo, 66*, 99–105.

Ferrari, J., Lior, N. & Slycke, J. (2003). An evaluation of gas quenching of steel rings by multiple-jet impingement. *J Mater Process Technol, 136*, 190–201.

He, Y., Mena, Y., Zhao, Y., Lu, H. & Ding, Y. (2009). Numerical investigation into the convective heat transfer of $TiO_2$ nanofluids flowing through a straight tube under the laminar flow conditions. *Appl Therm Eng, 29*, 1965–1972.

Manca, O., Ricci, D., Nardini, S., Di Lorenzo & G. (2016). Thermal and fluid dynamic behaviors of confined laminar impinging slot jets with nanofluids. Int Commun Heat Mass Transf 2016 ; 70:15–26.

Mookherjee, O., Pramanik, S. & Kumar Kar, U. (2020). Numerical investigation of a confined laminar jet impingement cooling of heat sources using nanofluids. *ASME J Heat Transfer, 142* (8), 082301.

Mosurkal, R., Samuelson, L.A., Smith, K.D., Westmoreland, P.R., Parmar, V.S. & Yan, F. (2008). Nanocomposites of $TiO_2$ and siloxane copolymers as environmentally safe flame retardant materials. *J Macromol Sci A Pure Appl Chem, 45*, 924–946.

Patankar, S.V. (1980). *Numerical heat transfer and fluid flow*. Hemisphere Publishing.

Rohsenow, W.M., Hartnett, J.P. & Cho, Y.I. (1998). *Handbook of heat transfer* (3rd edition). McGraw-Hill.

Selvakumar, P. & Suresh, S. (2012). Convective performance of CuO/water nanofluid in an electronic heat sink. *Exp Therm Fluid Sci, 40*, 57–63.

Venkitaraj, K.P, Suresh, S., Alwin M., T, Bibin, B.S & Abraham, J. (2018). An experimental investigation on heat transfer enhancement in the laminar flow of water/$TiO_2$ nanofluid through a tube heat exchanger fitted with modified butterfly inserts. *Heat Mass Transf, 54*, 813–829.

Xia, G.D., Liu, R., Wang, J. & Du M. (2016). The characteristics of convective heat transfer in microchannel heat sinks using $Al_2O_3$ and $TiO_2$ nanofluids. *Int Commun Heat Mass Transf, 76*, 256–264.

Yang, L., & Du, K. (2017). A comprehensive review on heat transfer characteristics of $TiO_2$ nanofluids. *Int sJ Heat Mass Tran, 108*, 11–31.

Zuckerman, N. & Lior, N. (2006). Jet impingement heat transfer: physics, correlations, and numerical modeling. Adv Heat Transfer, 39, 565–631.